

Supporting Information for- 2-Photon Tandem Device for Water Splitting: Design Parameters and Potential Feasibility

Brian Seger, Peter C. K. Vesborg, Ivano Castelli, Ole Hansen, Karsten W. Jacobsen and Ib Chorkendorff*

Email: ibchork@fysik.dtu.dk

Introduction:

In the introduction it was mentioned that there are thermodynamics losses that prohibits photovoltage from reaching the bandgap, thus forcing a loss of approximately 400 mV per semiconductor. This section goes into more detail explaining these losses.

In their seminal paper Shockley and Queisser¹ showed that the maximum thermodynamically allowed open circuit voltage, V_{oc} , of a photoabsorber with a band gap E_g , a refractive index n_r and a temperature T can be obtained from a detailed balance calculation, where the rate of absorbed photons is balanced by the rate of emitted photons and the rate of non-radiative recombination. If the solar spectrum is approximated by a blackbody spectrum at T_S the result is:

$$V_{oc} = \frac{E_g}{q} \left(1 - \frac{T}{T_S}\right) + \frac{kT}{q} \ln \frac{T_S}{T} - \frac{kT}{q} \left(\ln \frac{\Omega_{device}}{\Omega_{sun}} + \ln \frac{4n_r^2}{\tau} - \ln \frac{R_{rad}^{net}}{R_{rad}^{net} + R_{nonrad}} \right) \quad \text{Equation S1}$$

Where q is the elementary charge, k is Boltzman's constant, R_{rad}^{net} is the net radiative recombination rate and R_{nonrad} is the nonradiative recombine rate. In Equation S1 the first term is the band gap corrected by the Carnot efficiency term, the second term is a slight advantage gained by cooling the photons² and the terms in the brackets are entropic loss terms. The first entropic term arises since the solar radiation is incident from a quite small space angle Ω_{sun} ($\sim 6 \times 10^{-5}$), while luminescence from the absorber is emitted into the larger space angle Ω_{device} ($\sim \pi$) (i.e. the incident light only populates a few of the many optical modes in the absorber), the second term arises due to insufficient light trapping of the incident photons and therefore imperfect absorption (i.e. imperfect optical design, characterized by the light trapping coefficient $1 \leq \tau \leq 4n_r^2$), the last term is due to non-radiative recombination losses (i.e. imperfect material). Perfect absorber materials and good optical design may minimize or eliminate the last two loss terms, while solar concentration (or restriction of the emission space angle)³ can be used to reduce the first entropic loss term.

The detailed balance calculation can also be applied to conditions where a photocurrent is flowing and, in particular, the photovoltage V_{mp} at optimum output power becomes:

$$V_{mp} = V_{oc} - \frac{kT}{q} \ln \left(1 + \frac{qV_{mp}}{kT}\right) \approx V_{oc} - \frac{kT}{q} \ln \left(1 + \frac{qV_{oc}}{kT}\right) \quad \text{Equation S2}$$

where a penalty of approximately 100 mV has to be paid in addition to the approximately 300 mV from the space angle mismatch. This leads to the conclusions that even for perfect materials and perfect optical design the useful photovoltage to drive redox reactions including their overpotentials is approximately 400 mV less than the bandgap voltage at one sun irradiation.

Section 1: In Depth Explanation of the Photoanode, Photocathode, and their Interface

Photoanode

The photoanode needs to produce photogenerated holes that are at or more anodic than the potential needed to oxidize water to O_2 . This potential consists of the thermodynamic oxidation potential plus overpotentials, which is near 1.6V vs. RHE using optimal O_2 evolution catalysts.⁴

It is essential to realize that even though the hole may be located in the valence band, its thermodynamic potential (or hole quasi-Fermi level) will actually be located more cathodic than this. Any energy difference

between the valence band and the hole quasi-Fermi level is simply a loss in photoanode efficiency ($\eta_{PA,h}$). Figure S1 shows this loss as it relates to the photoanode bandgap ($E_{G,PA}$), the photovoltage (V_p), and $\eta_{PA,e}$. $\eta_{PA,e}$ is the loss that corresponds to the potential range from the electron quasi-Fermi level until the conduction band edge. In Figure S1 this corresponds to the difference between the photoanode conduction band and the red dotted line.

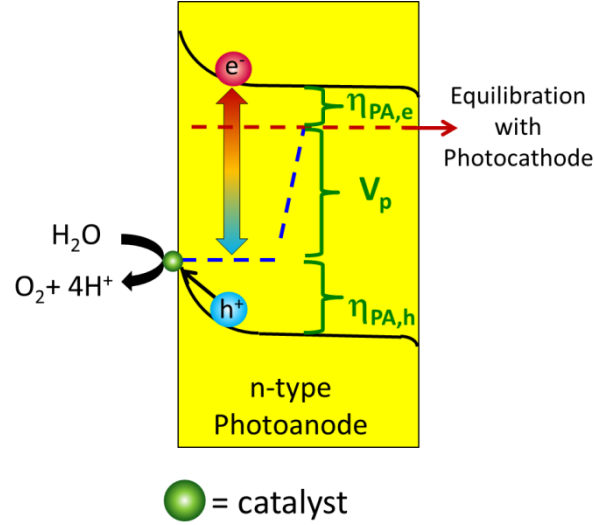


Figure S1: This figure shows the bandgap can be separated into 3 sections: losses between the valence band and hole quasi-Fermi level ($\eta_{PA,h}$), photovoltage (V_p), and losses between the electron quasi-Fermi level and the conduction band ($\eta_{PA,e}$).

To quantitatively describe $\eta_{PA,h}$ we must first start by defining the bandgap in terms of photovoltage and losses. Equation S3 does this.

$$qE_{G,PA} = \eta_{PA,h} + V_p + \eta_{PA,e} \quad \text{Equation S3}$$

The equation to determine photovoltage in a photovoltaic is given by Equation S4

$$V_p = \frac{nkT}{q} \ln \left(\frac{J_{L,PA} - J_{ox}}{J_{0,PA}} + 1 \right) \quad \text{Equation S4}$$

where n is an ideality factor (usually near 1), $J_{L,PA}$ is the anodic saturation current under photoirradiation, $J_{0,PA}$ is saturation current in the dark, which is a function of temperature, and J_{ox} is the oxidation current of an operating device. If 100% faradaic efficiency is assumed, J_{ox} corresponds to the O_2 evolution current. By inserting Equation S4 into Equation S3 and rearranging we are left with Equation S5.

$$\eta_{PA,h} = \frac{E_{G,PA}}{q} - \frac{nkT}{q} \ln \left(\frac{J_{L,PA} - J_{ox}}{J_0} + 1 \right) - \eta_{PA,e} \quad \text{Equation S5}$$

In semiconductor analysis it is mostly justified to approximate the Fermi-Dirac statistics by Boltzmann statistics, thus $\eta_{PA,e}$ would equal $kT/q \cdot \ln(N_c/N_d)$, where N_d and N_c are the donor density and effective density of states in the conduction band of the semiconductor, respectively. While it would appear this loss could be completely removed by increasing the donor density (N_d) until it approached N_c , increased doping density also increases the recombination rate of electrons and holes.

An increase in recombination leads to a decrease in $J_{L,PA}$ and an increase in J_0 from Equation S5. This then leads to a greater loss in $\eta_{PA,h}$ and/or a decrease in the O_2 evolution current. Thus a compromise needs to be made in choosing an N_d that helps maximize the 2nd term in Equation S5, but helps minimize the 3rd term. A way to get around the donor density compromise is to increase $J_{L,PA}$ through efficient hole transport to the surface via band

bending. Band bending within the semiconductor is a common strategy to maximize anodic current as discussed in the following paragraph.

In photocatalytic water splitting applications, the photoanode's interaction with water often pins the band position at the semiconductor-electrolyte interface. This simply means that the band positions will not change at this interface. Holes are thermodynamically favoured to move cathodically. Thus if the valence band in the bulk can be positioned more anodically than the pinned surface, holes will be favoured to diffuse to the surface to evolve O₂. The bulk band diagram of the photoanode is set such that the majority carrier Fermi-level will align with the photocathode's majority carrier Fermi level. If the majority carrier of the photoanode is electrons (i.e. n-type), by definition the holes, and hence the bulk valence band, will be more anodic than this. Thus an n-type photoanode is necessary to maximize band bending in the semiconductor. Figure 2 in the main paper demonstrates this principle. From Figure 2 it can also be seen that the equilibrated majority carrier Fermi level is a function of both photoabsorbers, thus the exact degree of band bending in the photoabsorber is a function of both photoabsorbers.

The preceding paragraph might lead one to believe the conclusion that the more cathodic the valence band is at the water-electrolyte interface, the greater the potential band bending, and hence the better the charge separation. While this is true to an extent, a situation could arise where the valence band at this interface is more cathodic than the potential where O₂ evolution takes place (i.e. 1.23 V vs. RHE + η_A where η_A is the O₂ evolution catalyst overpotential). In this case, when photogenerated holes have a quasi-Fermi level which is sufficiently anodic to evolve oxygen, the holes will move cathodically to the surface valence band. These holes would then need to fill all the density of states between valence band at the surface and the hole quasi-Fermi level. The vast amount of holes needed to fill up all the electronic states normally limits the increase in the surface valence band beyond the quasi-Fermi level to typically less than 100 mV. Thus it is probably of no benefit have the valence band located more cathodic than at the O₂ evolution potential. It follows that a near optimal valence band position at the surface-electrolyte interface $VB_{PA,surface}$ may be expressed by Equation S6.

$$VB_{PA,surface} = 1.23 \text{ V vs. RHE} + \eta_A$$

Equation S6

Equation S6 shows reasonable parameters necessary for an effective photoanode for water splitting. Using the best available catalysts ($\eta_A \approx 350 \text{ mV}$)⁴ the valence band should be located at $\sim 1.6 \text{ V vs. RHE}$. It should be noted that if the valence band is located 100 mV anodic of the potential where O₂ evolution occurs, band bending may decrease, thus moderately increasing $\eta_{PA,h}$. On the other hand if the valence band is located 100 mV more cathodic than the O₂ evolution potential, the semiconductor will be heavily in inversion mode and may not allow any holes to evolve O₂, thus completely killing the efficiency of the device. This means that if a material can't be found with the optimal valence band level, one should always look to materials with more anodic valence bands rather than more cathodic valence bands.

Even though there clearly will be inefficiencies within the photoanode due to recombination, etc., the equation to determine the parameter of the photoanode valence band (Equation S6) does not include such losses. If losses are not incorporated into the valence band potential at the surface, the question arises: Where are these losses at? The answer to this question is that these losses relate to the bulk valence band. Equation S7 shows the potential at which the bulk valence band ($VB_{PA,Bulk}$) needs to be located in order to efficiently split water.

$$VB_{PA,bulk} \geq 1.23 \text{ V vs. RHE} + \eta_A + \eta_{PA,h}$$

Equation S7

Equation S7 shows that it is the bulk valence band, not necessarily the valence band at the surface, which needs to be pushed more anodic. As mentioned earlier, the valence band at the surface of a given semiconductor material is normally set at the surface due to pinning effects, but the bulk of a semiconductor can vary. Thus this analysis has shown that in the quest to find a photoanode material with the proper parameters, only the thermodynamic water splitting potential and catalyst overpotential needs to be considered. Losses in photovoltage do not necessarily effect the optimal valence band location.

It should be noted that there are thermodynamic limits to how small $\eta_{PA,h}$ can be. If there are no losses due to $\eta_{PA,e}$, Equation S5 shows $\eta_{PA,h}$ reduces to the bandgap minus the photovoltage. From earlier in the supporting information these losses are derived to be no less than approximately 400mV. While these thermodynamic losses cannot be eliminated, it is possible to take advantage of them. The band bending in the semiconductor is simply the difference between $VB_{PA,bulk}$ and $VB_{PA,surface}$, which means the difference between Equation S6 and Equation S7. This means that $\eta_{PA,h}$ will basically be the band bending. Thus, the silver lining in these thermodynamic losses is that they can provide us with band-bending. Any further increase in $\eta_{PA,h}$ means an increased bandbending, which in turn increases the photovoltage, and thus partially decreases $\eta_{PA,h}$. This negative feedback loop helps dampen losses.

Another important aspect is stability in the dark. Since these devices will be in the dark at night, the photoanode must also be stable at the rest potential of the electrode in the dark. This is the potential where the solution, the LBG, and the SBG all are at equilibrium. This value is not easy to calculate because it depends on LBG and SBG dopant densities as well as electrolyte composition and concentration. However, if the H^+/H_2 redox couple dominates the overall system (which is probable because of much faster kinetics than O_2/H_2O), this potential may be close to 0 V vs. RHE which is very cathodic compared to normal operating conditions at the photoanode. It should be noted that in our stability calculations for our computationally screened photoabsorber/protection layer candidates, we did not include the dark situation since we could not accurately define what this potential should be.

Photocathode

Figure 2 shows that the photocathode will be the SBG for Design 1 and the LBG for Design 2. The goal of the photocathode is to produce a photogenerated electron that is sufficiently cathodic to evolve H_2 . The photocathode can be analysed in a similar manner as the photoanode. While thermodynamics allows this reaction to take place at 0.00 V vs. RHE (by definition), in reality an overpotential will once again be needed. The state of the art H_2 evolution (HER) catalysts have an overpotential (η_c) of approximately 50 mV in pH= 0 and 150 mV in pH= 14 (@ 10 mA/cm).^{2,5, 6} This means that the photogenerated electron must have a chemical potential (i.e. electron quasi-Fermi level) that is sufficiently cathodic to provide the overpotential.

In perfect analogy with the above discussion of holes in the photoanode, even though the photogenerated electron is located in the conduction band, its electron quasi-Fermi level will be located significantly anodic of this level. This difference between the conduction band and the electron quasi-Fermi level is simply a loss in the system, which we can denote as $\eta_{PC,e}$. To quantify this loss we can use an equation similar to Equation S5. By modifying Equation S5 for a photocathode instead of a photoanode, we get Equation S8.

$$\eta_{PC,e} = \frac{E_{G,PC}}{q} - \frac{kT}{q} n \times \ln\left(\frac{J_{L,PC} - J_{red}}{J_{0,PC}} + 1\right) - \eta_{PC,h} \quad \text{Equation S8}$$

Where $E_{G,PC}$ is the photocathode bandgap, $J_{L,PC}$ is the cathodic saturation current, $J_{0,PC}$ is the saturation current of the photocathode in the dark, J_{red} is the photoreduction current of an operating device and all other symbols have the same meanings as in Equation S5. If 100% faradaic efficiency is assumed J_{red} will correspond to the H_2 evolution current. Independent of faradaic efficiency, J_{red} will be the same magnitude of current as J_{ox} , but opposite in signs. This is fundamentally necessary to balance charge throughout the device.

$\eta_{PC,h}$ is the losses, which result from a difference between the photocathodes valence band and hole quasi-Fermi level. Since holes are the majority carrier in the photocathode, the $\eta_{PC,h}$ equals $kT/q \cdot \ln(N_v/N_a)$, where N_a is the acceptor density and N_v is the effective density of states in the valence band of the photocathode. An increase in acceptor density will decrease $\eta_{PC,h}$, but could potentially decrease $J_{L,PC}$ and increase $J_{0,PC}$ due to recombination issues. In parallel with the photoanode case, one of the main keys to increasing $J_{L,PC}$ (as well as increasing J_{red} and decrease $\eta_{PC,e}$) is to build band bending within the semiconductor.

Since electrons want to move more anodic, this means that the bulk conduction band needs to be more cathodic than the conduction band at the electrolyte surface. This will allow the photogenerated electrons to flow downhill in the semiconductor to the surface. The conduction band at the surface will most probably be pinned due to its interaction with water, thus the bulk conduction band must be forced more cathodic to allow for proper band bending. The bulk band positions can be forced to move by varying the potential of the majority carrier. Since the photocathode will be in electrical contact with the photoanode, this equilibrium will invariably change the potential of the majority carrier. If the majority carrier of the photocathode is holes (i.e. p-type), this will push the bulk conduction band more cathodic, thus allowing for the proper bandbending to force photogenerated electrons to the photocathode surface. Thus a photocathode must be p-type to allow proper band bending. Figure 2 in the main paper illustrates this by showing that the photocathode's majority carrier quasi-Fermi level (dotted blue line) aligns with the photoanodes majority carrier quasi-Fermi level (dotted red line), thus allowing for the photocathode's band bending.

The same reasoning used for determining an optimal photoanode valence band at the surface/electrolyte interface can be used for determining the optimal photocathode conduction band position. If the photocathode's conduction band is too cathodic it means that there is less than maximal band bending. Conversely, if the conduction band is too anodic the semiconductor will go into inversion mode and may limit the electron quasi-Fermi level. The optimum potential for the surface conduction band ($CB_{PC,surface}$) is thus the point at which the H_2 evolution occurs. Equation S9 expresses this parameter.

$$CB_{PC,surface} = 0.00 \text{ V vs. RHE} + \eta_c \quad \text{Equation S9}$$

$CB_{PC, Surface}$ corresponds to a material with conduction bands near -0.05 V vs. RHE at pH=0 using Pt or -0.15 V vs. RHE at pH= 14 using Pt-Ni.⁶ Since $CB_{PC, surface}$ is a material property, Equation S9 is a parameter constraint for any photocathode material. While Equation S9 describes the parameters needed for the conduction band at the surface, Equation S10 shows the necessary parameters needed for the conduction band in the bulk

$$CB_{PC, Bulk} = 0.00 \text{ V vs. RHE} + \eta_C + \eta_{PC} \quad \text{Equation S10}$$

Equation S10 shows that semiconductor inefficiencies will show up as a function of the necessary condition for the bulk conduction band rather than the necessary condition for the conduction band at the surface.

An effective photocathode must also be stable at the operating potentials used for H₂ evolution. As mentioned previously, the photocathode will most likely have to operate in highly acidic or highly basic conditions to prevent ohmic losses. Many materials corrode under such conditions, which eliminates many otherwise good candidates. Naturally, the photocathode also needs to be stable at the equilibrium potential during dark conditions, but again we did not take this into account in our stability calculations since this is a difficult to define parameter.

Photoanode/ Photocathode Interface

An important assumption that was made in discussing the photoanode and photocathode was that the majority carrier of the opposite photoabsorber would assist in band bending. However this assumption needs to be revisited. As an example, Figure S2 takes a simplified version of Design 1 from Figure 2 and shows the dark Fermi levels of the LBG and SBG before they equilibrate. In Figure S2A, there is no overlap between the band gaps of the photoabsorbers while in Figure S2B there is an overlap. When the 2 photoabsorbers are connected their majority Fermi levels align as shown in Figure S2C and S2D. Since it is assumed that the semiconductors' electrodes are pinned at the surface, the Fermi level equilibration produces band bending. In the case where the band gaps do not overlap (Figure S2C) the band bending is such that electrons will flow to the surface in the photoanode and holes will flow to the surface in the photocathode. That will not allow for photocatalytic water splitting! In the case where the semiconductors overlap (Figure S2D), the band bending is such that photogenerated electrons will flow to the photocathode's surface and holes to the photoanode's surface. This will allow for photocatalytic water splitting.

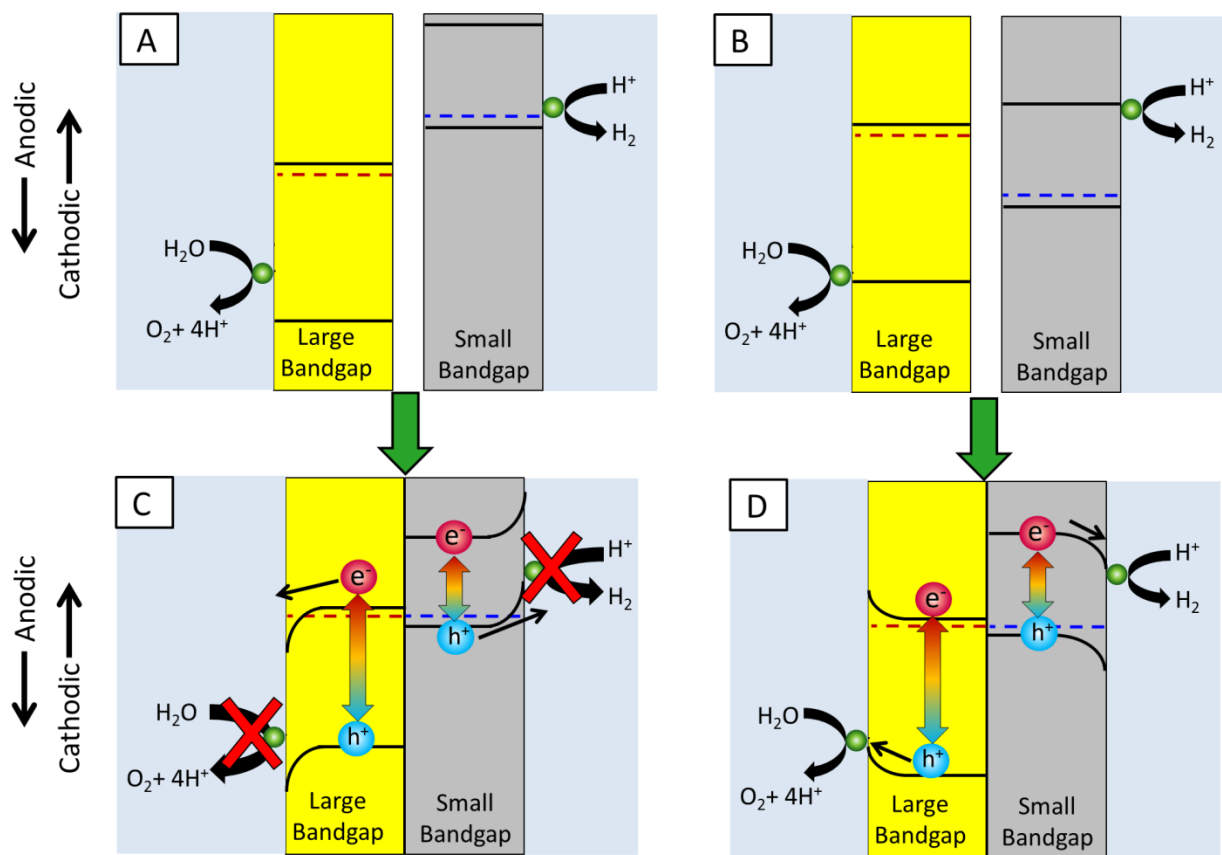


Figure S2: An unequilibrated 2-photoabsorber device A) without overlapping band and B) with overlapping bands. Figure C and D shows the band bending once A and B are equilibrated. Figure C and D also demonstrate which direction photogenerated electrons will travel in these devices.

It is evident that overlap between the photoabsorbers band gaps is necessary for correct band bending. Counter-intuitively, this means that the photoanode should have a relatively cathodic band structure while the photocathode should have a relatively anodic band structure. On the other hand, as was pointed out previously, having a photocathode band structure too anodic, or having a photoanode band structure too cathodic, could lead to inversion at the surface and the problems that come with it. Thus this needs to be avoided. It may have appeared that in order to increase band bending, a new constraint has been introduced on the position of the photoanode and photocathode. However one should note the conditions for an optimal photoanode valence band and photocathode conduction band can already be described by Equation S5 and Equation S9.

Once the device is photoirradiated, the inherent band bending and physical characteristics may entail that either the photocathode or photoanode may be more efficient at their respective redox reaction. For example, if the photoanode is more efficient, the photogenerated holes will be used for O₂ evolution, but there will be a build-up of photogenerated electrons (i.e. majority carriers). The build-up of majority carriers in the photoanode will push the equilibrated Fermi level of the photoanode-photocathode system more cathodic. This cathodic push of the majority carriers' Fermi level decrease band bending in the photoanode, but increase band bending in the photocathode. The equilibrated majority carrier level of the photoabsorber composite will continue to shift more cathodic until the band bending of the 2 photoabsorbers are such that they both produce equal amount of current (but opposite in sign). Thus one could say that a 2-photon water splitting device has a 'balancing mechanism' to help it optimize its efficiency.

Section 2: Screening of (Unprotected) Photoabsorber Candidates

Table S1 gives the raw results of the computational screening for calculating photoabsorber candidates. The materials highlighted in red were eliminated in the main work because they were experimentally shown not to have the correct electronic structure (see preceding paragraphs). The materials highlighted in blue were unfit for the given parameters, but was valid for a different pH/bandgap range. Thus in the main work they were shifted to a different design/pH/absorber section. With regards to bandgap, materials were only eliminated in their intrinsic (not extrinsic) bandgap was shown not to meet the specified conditions.

Table S1: Computational screening data for potential photoabsorber candidates for 2-photon water splitting devices.

Design	pH	Screening Parameters	Absorber (electrode)	# of Candidates	Candidate materials
Design 1	0	$1.5 \leq E_{\text{Gap}} \leq 2.1$ VB > 1.6 V vs. RHE	LBG (anode)	9	AuClO, Co(ReO ₄) ₂ , Cr ₂ Ag ₂ O ₇ , CuRhO ₂ , Mg(BiO ₃) ₂ , Zn(RhO ₂) ₂ , AuCl ₂ , Au ₂ O ₃ , InAuO ₂
		$0.9 \leq E_{\text{Gap}} \leq 1.5$ CB < 0.00 V vs. RHE	SBG (cathode)	13	As ₂ Os, As ₂ Ru, CdTe, FeSbS, GeAs, GeAs ₂ , NaTiCuS ₃ , KCuSe, SnSe, Te ₂ Mo, CdSe, GeTe, Te ₂ Ru
	14	$1.5 \leq E_{\text{Gap}} \leq 2.1$ VB > 1.6 V vs. RHE	LBG (anode)	21	Ag ₃ VO ₄ , AuClO, Au ₂ O ₃ , Ba ₂ FeMoO ₆ , Bi ^(III) ₃ Bi ^(V) O ₇ , Ca(RhO ₂) ₂ , CdHgO ₂ , Cd(RhO ₂) ₂ , Cd ₂ SnO ₄ , Co(ReO ₄) ₂ , Cr ₂ Ag ₂ O ₇ , CuRhO ₂ , Mg(BiO ₃) ₂ , Zn(RhO ₂) ₂ , Ag ₂ CO ₃ , AuCl ₂ , ClO ₂ , InAuO ₂ , InAgO ₂ , FeMoO ₄ , Sr ₂ FeWO ₆
		$0.9 \leq E_{\text{Gap}} \leq 1.5$ CB < 0.00 V vs. RHE	SBG (cathode)	1	Ca ₃ (CoO ₃) ₂
Design 2	0	$1.5 \leq E_{\text{Gap}} \leq 2.1$ CB < 0.00 V vs. RHE	LBG (cathode)	10	Cs ₂ Ni ₃ S ₄ , InSe, NaHfCuSe ₃ , NaPt ₂ Se ₃ , NaZrCuSe ₃ , SbIrS, WSe ₂ , MoSe ₂ , PbTe, PPdSe
		$0.9 \leq E_{\text{Gap}} \leq 1.5$ VB > 1.6 V vs. RHE	SBG (anode)	3	Bi ₂ Pt ₂ O ₇ , HfBrN, PtO ₂
		$1.5 \leq E_{\text{Gap}} \leq 2.1$ CB < 0.00 V vs. RHE	LBG (cathode)	2	NaPt ₂ Se ₃ , Sr ₂ FeWO ₆

	$0.9 \leq E_{\text{Gap}} \leq 1.5$ VB > 1.6 V vs. RHE	SBG (anode)	11	Bi ₂ Pt ₂ O ₇ , HfBrN, PtO ₂ , LaRhO ₃ , LiBiO ₃ , Ag ₂ BiO ₃ , Ag ₂ CO ₃ , AgF ₃ , Ba ₂ FeMoO ₆ , CuCl ₂ , Sb ₂ WO ₆
--	----------------------------------------------------------	----------------	----	-------------------------------------------------------------------------------------------------------------------------------------------------------------------------------------------------------------------------------------------------------------------------------------------------------------

Design 1, pH= 0 LBG: Au₂O₃ is soluble in acid.⁷ AuCl₂ is only stable in SOCl₂.⁸ The reference for the InAuO₂ in the Materials Project Database referred to a theoretical InAuO₂.⁹ We have been unable to find any literature experimentally producing this material. Since this analysis is only scanning experimentally produced materials, we eliminate this as a potential candidate.

Design 1, pH=0 SBG: CdSe has a bandgap of 1.74 eV, thus it was moved to Design 2, pH=0, LBG.¹⁰ Te₂Ru was eliminated because its bandgap is known to be 0.5 eV or less depending upon temperature.¹¹ GeTe was eliminated due to its small bandgap 0.6 eV.¹²

Design 1, pH=14 LBG: AuCl₂ and InAuO₂ were eliminated for the same reasons as for Design 1, pH=0. InAgO₂ was eliminated for the same reason as InAuO₂.⁹ ClO₂ is a gas at room temperature.¹³ Ag₂CO₃ is slightly soluble in water ~30 mg/L.¹⁴ FeMoO₄ is known to have a bandgap of 4.0 eV.¹⁵ Sr₂FeWO₆ has a bandgap of 0.1 eV.¹⁶

Design 1, pH=14 SBG: No candidates were eliminated

Design 2, pH=0 LBG: MoSe₂ is known to have a bandgap near 1.3 eV,¹⁷ thus it would more appropriately be placed in Design 1, pH=0, SBG. PbTe has a bandgap of 0.3 eV.¹⁸ PPdSe has a bandgap of 0.7 eV.¹⁹

Design 2, pH=0 SBG: No candidates were eliminated

Design 2, pH=14 LBG: Sr₂FeWO₆ has a bandgap of 0.1 eV.²⁰

Design 2, pH=14 SBG: LaRhO₃ is known to have a conduction band more cathodic than the H⁺/H₂ redox potential and have a bandgap of 1.35 eV.²¹ Thus it would be more appropriately placed in Design 1, pH=14, SBG. LiBiO₃ is known to have a bandgap of 1.8 eV,²² thus it would more appropriately be placed in Design 1, pH=14, LBG. Ag₂BiO₃ has a bandgap of 0.7 eV.²³ Ag₂CO₃ is slightly soluble in water ~30 mg/L.¹⁴ Sb₂WO₆ has a bandgap of 2.5 eV.²⁴ CuCl₂ is soluble in water.⁷ AgF₃ is thermodynamically unstable.²⁵

Section 3: Analysis on Pillared Structures

Figure S3 shows a diagram of a pillared device. In this case one can see that both redox catalysts could inadvertently absorb light, which would leave less light to be absorbed in the LBG and SBG. However, since the LBG catalyst is closer to the irradiation side, it carries the risk to decrease efficiency more than the SBG-side catalyst. Furthermore by the time the light reaches the SBG, all the high energy photons should have already been absorbed (i.e. $h\nu > \sim 1.7$ eV) by the LBG. ($h\nu$ stands for photon energy.) Thus only in the range of $SBG < h\nu < LBG$ will the SBG catalyst's light absorption negatively impact device current. It should be noted that protection layers would also interfere with light absorption in a manner similar to redox catalysts.

One unique condition that occurs due to pillared structures is that a semiconducting protection layer on the SBG side would need to have a bandgap as big or larger than the LBG to guarantee the SBG protection layer would not interfere with the SBG photoabsorber's light absorption. Quantitatively, the SBG protection layer should then be larger than ~ 1.7 eV in an optimal device. Materials such as MoS_2 ($E_g = 1.75$ eV and a conduction band near 0.0 V vs. RHE)²⁶ for a CPL and BP ($E_g = 2.0$ eV, valence band 1.44 V vs. RHE)²⁷ for an APL fit these conditions thus adding flexibility in the pool of potential SBG protection layer candidates.

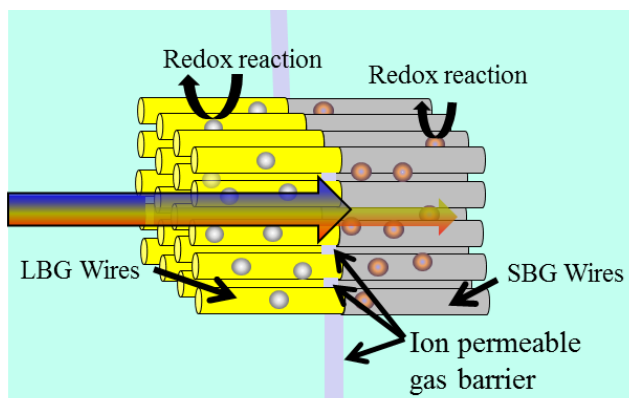


Figure S3: This figure shows a pillared approach to a 2-photon water splitting devices. The redox reactions of the photoabsorbers are either the H^+/H_2 reaction or the H_2O/O_2 reaction. Which reaction takes place on which photoabsorber depends on whether a Design 1 or Design 2 approach is used (See Figure 2 in main paper).

Section 4: Screening of Anode Protection Layers (APL)

Table S2 gives the raw results of the computational screening for anode protection layers (APL). The screening parameters used were that the material had to be stable in O₂ evolving conditions (1.23-1.8 V vs. RHE), have a relatively cathodic valence band (1.1 V vs. RHE < VB < 1.8 V vs. RHE), and have a bandgap larger than 3.0 eV. The materials highlighted in red have been experimentally shown to have a bandgap less than 3.0 eV.

Table S2: Computational screening data for potential photoabsorber candidates for 2-photon water splitting devices.

Design	pH	# of Candidates	Candidate materials
Design 1	0	0	
	14	2	Sr₂PbO₄ , Ca ₄ PdO ₆

Design 1, pH=14: Sr₂PbO₄ has too small of a bandgap (~1.8 eV).²⁸ However this materials bandgap is large enough to potentially allow it to help protect SBG photoanodes if a pillared type structruing. (This is on the condition that the theoretical valence band position is accurate.)

Section 5: Screening of Protected Photoabsorber Candidates

Table S3 gives the raw results of the computational screening for protected photoabsorbers where a p-n junction is used. Thus the only screening parameters used were that the material had to have the correct bandgap for either a large bandgap material (LBG) or a small bandgap material (SBG). The materials highlighted in blue were moved to a different section that appropriately matches their experimentally proven characteristics. The materials highlighted in red were removed from the potential candidates either due to a wrong bandgap or they were not thermodynamically stable.

Table S3: Computational screening data for potential protected photoabsorber candidates for 2-photon water splitting. devices.

Design	Screening Parameters	# of Candidates	
SBG	$0.9 \leq E_{\text{Gap}} \leq 1.5$	58	BaAs ₂ , BaCaSn, Ba ₂ Cu(PO ₄) ₂ , Ba ₂ FeMoO ₆ , Ba ₃ (Si ₂ P ₃) ₂ , BaLaI ₄ , Ba ₃ P ₄ , CaBaSi, Ca ₃ (CoO ₃) ₂ , Ca ₂ Si, Ca ₃ SiO, CoAsS, CuCl ₂ , CuP ₂ , FeSbS, K ₂ Mo ₆ S ₆ , KNbS ₂ , KPb, KSnAs, KZnAs, LaAs ₂ , LaZnAsO, LaS ₂ , MgP ₄ , MnP ₄ , Na ₄ FeO ₃ , Na ₄ FeO ₄ , NaNbS ₂ , NaNiO ₂ , NaSnP, NaTiCuS ₃ , NaTiS ₂ , NaZnP, NbFeSb, NbI ₃ O, Si, Sr ₂ As ₂ , Sr ₃ As ₄ , SrCaSi, SrCaSn, SrLaI ₄ , Sr(ZnP) ₂ , V(S ₂) ₂ , Zn ₂ Cu(AsO ₄) ₂ , ZrBr ₃ , ZrCl ₂ , ZrCl ₃ , Cu₂O , LaZnPO , Ba₂CuO₂Cl , FeSi₂ , FeP₂ , I₄(SbF₆)₂ , Mg₃Sb₂ , NaSb , Sb₂WO₆ , Sr₂Si , TiCoSb , Ti₂Nb₆O₁₂
LBG	$1.5 \leq E_{\text{Gap}} \leq 2.1$	61	B, BP, BaCuN, BaCu ₂ SnS ₄ , Ba(MgSb) ₂ , BaP ₃ , Ba ₄ Sb ₂ O, Ba ₂ ZnN ₂ , Ca ₃ AlAs ₃ , Ca(BC) ₂ , Ca ₃ (BN ₂)N, Ca(MgSb) ₂ , CaNa ₁₀ Sn ₁₂ , Ca ₃ VN ₃ , Ca(ZnP) ₂ , CoBr ₂ , CuSbS₂ , Cu ₃ VS ₄ , FeBr ₂ , Fe(SiP) ₄ , FeSO ₄ , I ₂ , K ₃ As, K ₂ Ni ₃ S ₄ , K ₄ P ₆ , K ₃ Na ₂ SnAs ₃ , K ₂ NiAs ₂ , KSb, KV(CuS ₂) ₂ , KZnP, KCuZrS ₃ , MgAs ₄ , NaCuO ₂ , NaNbN ₂ , NaP, NaSbS ₂ , Nb ₆ F ₁₅ , NbI ₅ , SnZrS ₃ , SrP, Sr ₃ P ₄ , SrPbO ₃ , TiBrN, TiI ₄ , TiNCl, Sn ₂ TiO ₄ , WBr ₆ , ZnSiAs ₂ , ZrCl ₂ , Zr ₂ SN ₂ , FeS₂ , Na₃Sb , SnS , Sr₃SbN , ClO₂ , FeMoO₄ , LaI₂ , NaO₃ , NbCl₄ , PbS , Sr₂FeWO₆

SBG: Cu₂O has a bandgap of 2.0 eV,²⁹ and LaZnPO has a bandgap of 1.7 eV,³⁰ thus these materials are placed in the LBG group in the main paper. Ba₂CuO₂Cl was removed because it has never been experimentally produced and isolated due to its instability.³¹ FeSi₂ has a bandgap of 0.85 eV at room temperature.³² Mg₃Sb₂ is controversial in that Ahmadpour et. al found a bandgap of 0.21 eV,³³ whereas Busch et. al found a value of 0.8 eV.³⁴ Either way the bandgap is too small to be a SBG, thus it was eliminated. I₄(SbF₆)₂ has never been experimentally produced and isolated.³⁵ The following materials had an improper bandgap: FeP₂ (0.37 eV),³⁶ Mg₃Sb₂ (0.21 eV),³³ NaSb (0.8 eV),³⁷ Sb₂WO₆ (2.45 eV),²⁴ Sr₂Si (0.35 eV),³⁸ TiCoSb (0.19 eV),³⁹ and Ti₂Nb₆O₁₂ (0.3 eV).⁴⁰

LBG: CuSbS₂ has been reported to have bandgaps both in the SBG and LBG range^{41, 42}; however for this analysis we will consider it a LBG material. The following materials have bandgap that would make them SBG candidates: FeS₂ (0.9 eV),^{43, 44} Na₃Sb (1.1 eV),⁴⁵ SnS (1.1-1.3 eV),⁴⁶ and Sr₃SbN (1.15 eV).⁴⁷ Thus in the main paper these 4 materials are located under SBG. ClO₂, was discarded from the list because it is a gas at room temperature. The following materials has an improper bandgap for either a LBG or an SBG: FeMoO₄ (4.0 eV),¹⁵ and LaI₂

(metallic),⁴⁸ PbS (~0.3 eV),⁴⁶ and Sr₂FeWO₆ (0.1 eV).²⁰ NaO₃ is slightly unstable at standard temperatures and pressures,⁴⁹ and NbCl₄ has a bandgap that is too small.⁵⁰

(Photoabsorber) Semiconductor – (Protection Layer) Semiconductor Interface

When two semiconductors come into contact the conduction bands (valence bands) will align to give a band offset/discontinuity, Φ_b , as described by Equation S11

$$\Phi_b = (\chi_{PL} - \Phi_{CNL,PL}) - (\chi_{PA} - \Phi_{CNL,PA}) + S_{PL}(\Phi_{CNL,PL} - \Phi_{CNL,PA}) \quad \text{Equation S11}$$

where χ is the electron affinity (i.e. the energy difference between the vacuum level and the conduction band) and Φ_{CNL} is the charge neutrality level (CNL) for either the protection layer (PL) or the photoabsorber (PA). S is a factor between 0 and 1 indicating the degree to which the CNL has an effect in forming a microscopic interface dipole.⁵¹ The dipole arise due to the electronic states in the valence and/or conduction band of the SBG which have been projected into the bandgap regime of the LBG to form localized states. This is often referred to as metal induced gap states (MIGS). See Robertson for a more detailed description of the CNL.⁵¹ The semiconductor protection layers need to have a large bandgap to allow light to pass through. Louie et. al has shown that the S value of large bandgap semiconductors approach 1.⁵² This means that Equation 11 can be approximated for our situations as shown in Equation S12.

$$\Phi_b = \chi_{PL} - \chi_{PA} \quad \text{Equation S12}$$

Figure S4 shows diagrams for the case of three different barrier height situations for the photocathode-semiconducting protection layer interface. Figure S4A shows a negative barrier height, which creates a potential well at the semiconductor interface. This would mean the photoabsorber would have to go into inversion mode to transfer electrons to the surface. Surfaces are areas of high electron-hole recombination sites, thus going into inversion mode could significantly hurt efficiency. Figure S4B shows a positive barrier height, which could potentially allow increased electron hole separation, however this is only a local effect. Figure S4B shows that the positive barrier height effectively decreases band bending, thus this is not an optimal situation. Figure S4C shows that no barrier height is the optimal situation. Since the optimal band position of the cathode protection layer is set by its interaction with the electrolyte (Section 4), this also sets the optimal band position of photocathode. An analogous analysis can also be done for the case of the photoanode. In this case the optimal photoanode valence band position will be set by the optimal anode protection layer valence band position.

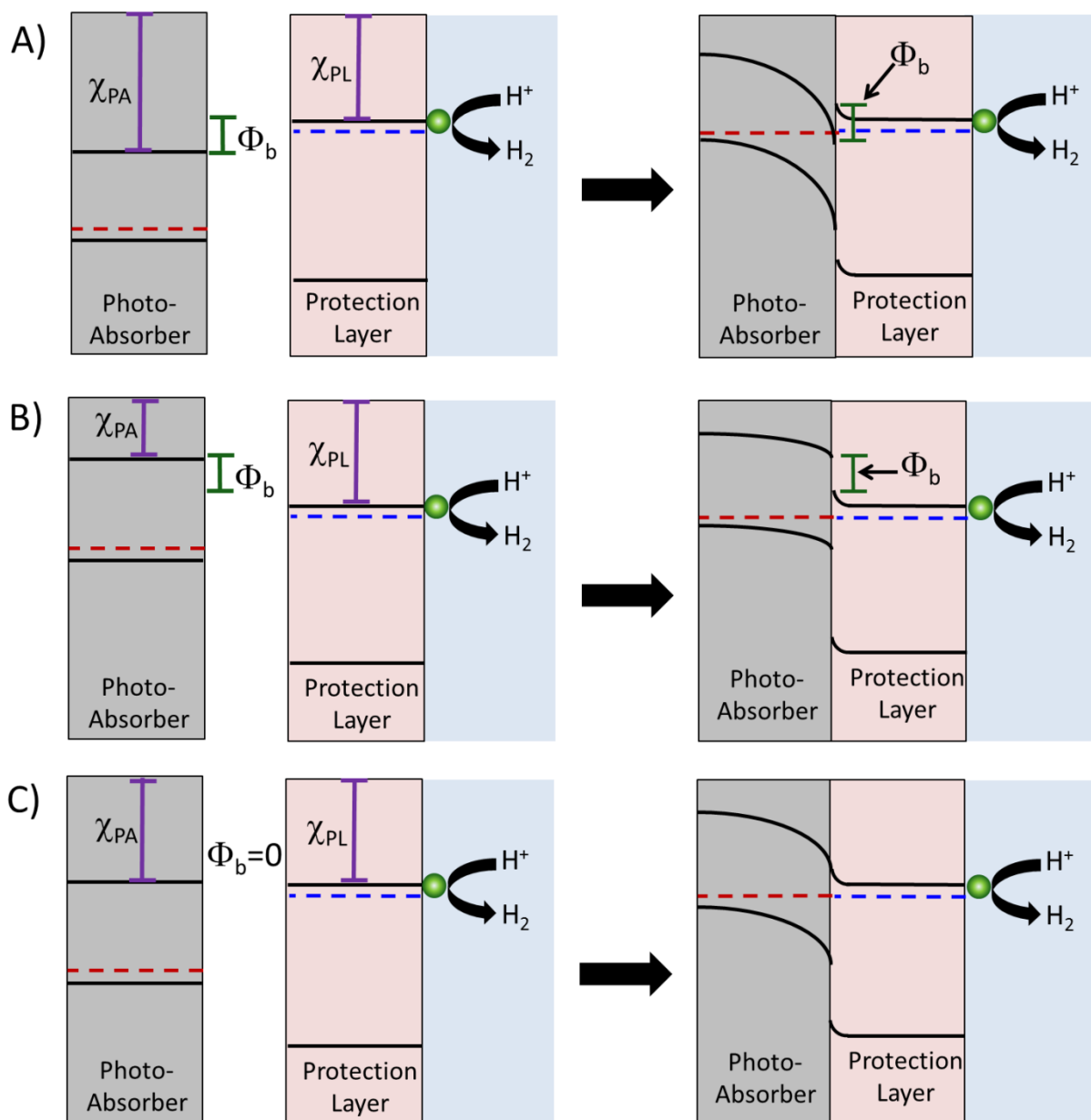


Figure S4: Energy diagrams showing semiconductor-semiconductor interfaces for three different barrier height situations. In all of the Figure S4's it is assumed that the donor density of the protection layer is orders of magnitude higher than in the photoabsorber, thus the majority of the band bending takes place within the photoabsorber.

Computational screening was done for finding photoanodes using the optimal valence band position for an APL as a cathodic limit for the valence band condition (i.e. $VB > 1.6$ V vs. RHE). For the photocathodes the optimal conduction band position for the CPL was used as an anodic limit (i.e. $CB < 0.0$ V vs. RHE). Table S4 shows the raw computational screening of abundantly available photoabsorbers that could be used with a semiconducting protection layer. If photoabsorbers containing rare materials were also included, computational screening showed that Design 1 would have 94 candidates for the LBG, and 30 for the SBG whereas Design 2 would have 19 for the LBG and 50 for the SBG. The color coding in the same as in Table 3. Since Table 4 is just a more filtered version of Table 3, there is no need to re-discuss the individual materials.

Table S4: Computational screening data for potential photoabsorber candidates for 2-photon water splitting devices by using either a semiconductor or insulating protection layer with no internal o-n junction.

Design	Photo-Absorber	Screening Parameters	# of Candidates	Candidates
1	LBG (Photoanode)	$1.5 \leq E_{\text{Gap}} \leq 2.1$ $\text{VB} > 1.6 \text{ V vs. RHE}$	22	CoBr ₂ , CuSbS ₂ , FeBr ₂ , FeSO ₄ , I ₂ , Nb ₆ F ₁₅ , NbI ₅ , SnZrS ₃ , TiBrN, TiI ₄ , TiNCl, Sn ₂ TiO ₄ , WBr ₆ , ZrCl ₂ , ZrCl ₃ , Zr ₂ SN ₂ , FeS ₂ , ClO ₂ , FeMoO ₄ , NaO ₃ , NbCl ₄ , Sr ₂ FeWO ₆
1	SBG (Photocathode)	$0.9 \leq E_{\text{Gap}} \leq 1.5$ $\text{CB} < 0.0 \text{ V vs. RHE}$	7	BaLaI ₄ , CuP ₂ , FeAs ₂ , FeSbS, MgP ₄ , Ba ₂ CuO ₂ Cl, FeP ₂
2	LBG (Photocathode)	$1.5 \leq E_{\text{Gap}} \leq 2.1$ $\text{CB} < 0.0 \text{ V vs. RHE}$	4	CuSbS ₂ , NaCuO ₂ , Zr ₂ SN ₂ , SnS
2	SBG (Photoanode)	$0.9 \leq E_{\text{Gap}} \leq 1.5$ $\text{VB} > 1.6 \text{ V vs. RHE}$	11	Ba ₂ Cu(PO ₄) ₂ , Ba ₂ FeMoO ₆ , CuCl ₂ , CuP ₂ , NbI ₃ O, V(S ₂) ₂ , Zn ₂ Cu(AsO ₄) ₂ , Sb ₂ WO ₆ , Ti ₂ Nb ₆ O ₁₂

Section 4 shows that a protection layer could be quite effective at a relatively large range of potentials (-0.4-0.2 V vs. RHE for a CPL and 1.1-1.8 V vs. RHE for an APL). This means Table S4 could actually include different materials if an efficient protection layer was found that had a band position not located exactly at either the H₂ or O₂ reaction potential. Therefore Table S4 (and Table 3 in the main paper) are more of an example set of parameters and materials rather than the only materials possible.

(Photoabsorber) Semiconductor – (Protection Layer) Insulator Interface

Since insulators are simply semiconductors with very large bandgaps, the band alignment will follow the same analysis as in the previous discussion on semiconductor-semiconductor interfaces. Since the bandgaps for insulators are even larger than that for semiconducting protection layers, the approximation that S equals 1 and the CNL has no influence on the band alignment is even more accurate. Using Equation S12 an insulator protecting layer will always give a high barrier height. (This is how we define an insulator in this work.) In the insulating case the electrons will not overcome the barrier height like the semiconducting case, but rather electronically tunnel through the material. Thus from an electronic standpoint and bandbending standpoint, it is as if the insulating layer is not there. If it is assumed that the valence and conduction band positions of the insulating protection layers shift with pH the same as the unprotected photoabsorber would, the system could be analyzed as if the photoabsorber is in direct contact with the electrolyte. This would allow us to use the analysis for the unprotected photoabsorbers to determine the optimal photoabsorber band positions. The band position parameters used in Table S4 are very similar to that of the unprotected case, thus this table can also give a good approximation of potential photoabsorber candidates using an insulating protection layer and no p-n junction. (The only difference in conditions between Table S4 and the unprotected case is a slight variation in conduction band potential.)

1. W. Shockley and H. J. Queisser, *Journal of Applied Physics*, 1961, **32**, 510-519.
2. T. Markvart, *Physica Status Solidi a-Applications and Materials Science*, 2008, **205**, 2752-2756.
3. A. Polman and H. A. Atwater, *Nature Materials*, 2012, **11**, 174-177.
4. C. C. L. McCrory, S. Jung, J. C. Peters and T. F. Jaramillo, *Journal of the American Chemical Society*, 2013, **135**, 16977-16987.
5. B. Seger, T. Pedersen, A. B. Laursen, P. C. K. Vesborg, O. Hansen and I. Chorkendorff, *Journal of the American Chemical Society*, 2013, **135**, 1057-1064.
6. R. Subbaraman, D. Tripkovic, D. Strmcnik, K.-C. Chang, M. Uchimura, A. P. Paulikas, V. Stamenkovic and N. M. Markovic, *Science*, 2011, **334**, 1256-1260.

7. W. M. L. D. R. Haynes, *CRC handbook of chemistry and physics : a ready-reference book of chemical and physical data*, CRC Press, Boca Raton, Fla., 2011.
8. D. B. Dellamico, F. Calderazzo, F. Marchetti and S. Merlino, *Journal of the Chemical Society-Dalton Transactions*, 1982, 2257-2260.
9. H. C. Kandpal and R. Seshadri, *Solid State Sciences*, 2002, **4**, 1045-1052.
10. V. V. Sobolev, V. I. Donetskikh and E. F. Zagainov, *Soviet Physics Semiconductors-Ussr*, 1978, **12**, 646-652.
11. P. C. Liao, J. K. Huang, Y. S. Huang and T. R. Yang, *Solid State Communications*, 1996, **98**, 279-282.
12. R. Tsu, W. E. Howard and L. Esaki, *Physical Review*, 1968, **172**, 779-&.
13. R. I. Derby and W. S. Hutchinson, *Inorganic Syntheses*, 1953, **4**, 152-158.
14. W. Holmes, *Anatomical Record*, 1943, **86**, 157-187.
15. Y. P. Yadava and R. A. Singh, *Journal of Materials Science*, 1986, **21**, 2825-2829.
16. S. Ray, A. Kumar, S. Majumdar, E. V. Sampathkumaran and D. D. Sarma, *Journal of Physics-Condensed Matter*, 2001, **13**, 607-616.
17. S. Chandra, D. P. Singh, P. C. Srivastava and S. N. Sahu, *Journal of Physics D-Applied Physics*, 1984, **17**, 2125-2138.
18. S. V. Kershaw, A. S. Sussha and A. L. Rogach, *Chemical Society Reviews*, 2013, **42**, 3033-3087.
19. T. A. Bither, P. C. Donohue and H. S. Young, *Journal of Solid State Chemistry*, 1971, **3**, 300-&.
20. N. E. Massa, J. A. Alonso, M. J. Martinez-Lope and M. T. Casais, *Physical Review B*, 2005, **72**.
21. H. Yoneyama, T. Ohkubo and H. Tamura, *Bulletin of the Chemical Society of Japan*, 1981, **54**, 404-407.
22. R. Ramachandran, M. Sathiya, K. Ramesha, A. S. Prakash, G. Madras and A. K. Shukla, *Journal of Chemical Sciences*, 2011, **123**, 517-524.
23. S. Deibele and M. Jansen, *Journal of Solid State Chemistry*, 1999, **147**, 117-121.
24. J. H. Bi, Y. Q. Liu, S. J. Liang, W. M. Wu, R. S. Yuan and L. Wu, *Journal of Nanoparticle Research*, 2013, **15**.
25. B. Zemva, K. Lutar, A. Jesih, W. J. Casteel, A. P. Wilkinson, D. E. Cox, R. B. Vondreele, H. Borrmann and N. Bartlett, *Journal of the American Chemical Society*, 1991, **113**, 4192-4198.
26. H. Tributsch and J. C. Bennett, *Journal of Electroanalytical Chemistry*, 1977, **81**, 97-111.
27. A. Goossens, E. M. Kelder, R. J. M. Beeren, C. J. G. Bartels and J. Schoonman, *Berichte Der Bunsen-Gesellschaft-Physical Chemistry Chemical Physics*, 1991, **95**, 503-510.
28. R. P. Diez, E. J. Baran, A. E. Lavat and M. C. Grasselli, *Journal of Physics and Chemistry of Solids*, 1995, **56**, 135-139.
29. A. Paracchino, N. Mathews, T. Hisatomi, M. Stefik, S. D. Tilley and M. Gratzel, *Energy & Environmental Science*, 2012, **5**, 8673-8681.
30. K. Kayanuma, R. Kawamura, H. Hiramatsu, H. Yanagi, M. Hirano, T. Kamiya and H. Hosono, *Thin Solid Films*, 2008, **516**, 5800-5804.
31. T. Kodenkandath, G. Calestani and F. C. Maticotta, *Journal of Materials Chemistry*, 1996, **6**, 1575-1578.
32. Z. Yang, K. P. Homewood, M. S. Finney, M. A. Harry and K. J. Reeson, *Journal of Applied Physics*, 1995, **78**, 1958-1963.
33. F. Ahmadpour, T. Kolodiaznyh and Y. Mozharivskyj, *Journal of Solid State Chemistry*, 2007, **180**, 2420-2428.
34. G. Busch, F. Hulliger and U. Winkler, *Helvetica Physica Acta*, 1954, **27**, 249-258.
35. R. Faggiani, R. J. Gillespie, R. Kapoor, C. J. L. Lock and J. E. Vekris, *Inorganic Chemistry*, 1988, **27**, 4350-4355.

36. G. Boda, B. Carlsson, O. Beckman, Stenstro.B, Rundqvis.S and V. Sagredo, *Physica Scripta*, 1971, **4**, 132-&.
37. R. Suhrmann and C. Kangro, *Naturwissenschaften*, 1953, **40**, 137-138.
38. J. Hu, A. Kato, T. Sadoh, Y. Maeda, K. N. Galkin, T. V. Turchin and H. Tatsuoka, *International Journal of Modern Physics B*, 2010, **24**, 3693-3699.
39. Y. Stadnyk, Y. Gorelenko, A. Tkachuk, A. Goryn, V. Davydov and O. Bodak, *Journal of Alloys and Compounds*, 2001, **329**, 37-41.
40. R. Allmann, A. I. Baumann, E. Hellner, H. Rosch and A. Kutoglu, *Naturwissenschaften*, 1964, **51**, 263-&.
41. Y. Rodriguez-Lazcano, M. T. S. Nair and P. K. Nair, *Journal of Crystal Growth*, 2001, **223**, 399-406.
42. C. Yan, Z. H. Su, E. N. Gu, T. T. Cao, J. Yang, J. Liu, F. Y. Liu, Y. Q. Lai, J. Li and Y. X. Liu, *Rsc Advances*, 2012, **2**, 10481-10484.
43. A. Ennaoui and H. Tributsch, *Solar Energy Materials*, 1986, **14**, 461-474.
44. G. Smestad, A. Ennaoui, S. Fiechter, H. Tributsch, W. K. Hofmann, M. Birkholz and W. Kautek, *Solar Energy Materials*, 1990, **20**, 149-165.
45. H. Jacobs and B. Hellmann, *Journal of Alloys and Compounds*, 1993, **191**, 51-52.
46. W. H. Strehlow and E. L. Cook, *Journal of Physical and Chemical Reference Data*, 1973, **2**, 163-200.
47. F. Gabler, M. Kirchner, W. Schnelle, U. Schwarz, M. Schmitt, H. Rosner and R. Niewa, *Zeitschrift Fur Anorganische Und Allgemeine Chemie*, 2004, **630**, 2292-2298.
48. J. D. Corbett, R. A. Sallach and D. A. Lokken, *Advances in Chemistry Series*, 1967, 56-&.
49. M. Jansen and H. Nuss, *Zeitschrift Fur Anorganische Und Allgemeine Chemie*, 2007, **633**, 1307-1315.
50. H. Schafer, W. Loose and B. Monheim, *Zeitschrift Fur Anorganische Und Allgemeine Chemie*, 1985, **522**, 99-107.
51. J. Robertson, *Journal of Vacuum Science & Technology A*, 2013, **31**.
52. S. G. Louie, J. R. Chelikowsky and M. L. Cohen, *Physical Review B*, 1977, **15**, 2154-2162.